Applied Radiation and Isotopes 118 (2016) 238–245

Contents lists available at ScienceDirect

Applied Radiation and Isotopes

journal homepage: www.elsevier.com/locate/apradiso

# Determination of the conventional true value of gamma-ray air kerma in a minitype reference radiation

Yixin Liu[a,b], Biao Wei[b], Renhong Zhuo[a], Dezhi Wen[a], Dajie Ding[a], Yang Xu[a,b], Benjiang Mao[a,*]

[a] Institute of Nuclear Physics and Chemistry, China Academy of Engineering Physics, Mianyang 621999, PR China
[b] Key Laboratory of Optoelectronics Technology and System, Ministry of Education, Chongqing University, Chongqing 400044, PR China

ARTICLE INFO

*Keywords:*
Air kerma
Reference radiation
Calibration
Principal component analysis
Support vector machine

ABSTRACT

To develop mobile calibration equipment for gamma-ray dose or dose rate meters in the field of radiation protection, a minitype reference radiation (MRR) of 0.5 m×0.5 m×0.5 m cube was set up and used for investigation. Two types, which add up to 12 daily used gamma-ray dose rate meters, were used as samples to determine the conventional true value of air kerma (CAK) at the point of test in the MRR. A gamma-ray spectrometer was also used to monitor the scattering gamma rays in the MRR, which were applied further to characterize the disturbance of scattering gamma ray in CAK determination. On the basis of the sample data sets of CAKs, scattering gamma spectra and air kerma values at the point of test without sample meters, a CAK prediction model at the point of test was developed by the least square support vector machine, which is a multiple nonlinear regression method. For reducing the amount of data and improving the regression efficiency, principal component analysis (PCA) was used to extract feature components from the scattering gamma-ray spectra before regression. A relative standard uncertainty of 4.65% was achieved in determining CAK in the MRR using the constructed prediction model.

## 1. Introduction

For calibrating dose or dose rate meters, the conventional true value of gamma-ray air kerma (CAK) is a key quantity value. Its determination method and the gamma-ray standard reference radiation (SRR) are regulated in the ISO 4037 series (ISO-4037-1:1996, 1996; ISO-4037-2:1997, 1997). The minimal space of a regulated SRR is not smaller than 4 m(L)×4 m(W)×3 m(H), which is kept to avoid the disturbance of the scattering gamma ray originating from the SRR inner surroundings in determining CAK accurately (JJG393, 2003). Considering the dimension of an SRR and its heavy weight because of the concrete shield, moving an entire SRR is impossible. Therefore, all dosimeters must be normally sent to a fixed calibration facility equipped with an SRR for calibration. However, for dosimeters fixed/installed in a nuclear facility or those needed to be calibrated in the field for some special situations, there is no appropriate method or tool to execute calibration (Minniti and Seltzer, 2007).

To meet the needs of calibrating dosimeters in situ or in the field, we proposed an idea on a mobile calibration technology and conducted a feasibility study. The technology was realized on a minitype reference radiation (MRR) with an isotope cesium-137 irradiator and by using sample dosimeters. The CAK at the point of test in an MRR was determined by constructing a CAK prediction model. The technical procedure of this technology is illustrated in Fig. 1.

Compared with an SRR, the MRR showed nonnegligible scattering gamma ray caused by the MRR's inner wall and the probe surface of the calibrated dosimeter, which may lead to an increase in CAK up to 13.4% and 8.9%,respectively, with or without a probe placed in it in our previous work. It is very difficult to correct the interference of scattering components accurately in measuring the CAK experimentally in an MRR or correct it in a normal way, because of its variation with the probe placed and the gamma-ray irradiation intensity. The energy response of the calibrated dosimeter should also be corrected for the difference and variation in gamma-ray components in an MRR compared with an SRR, which will cause variation in the indication value $R_{ij}$. Overall, determining the CAK or $K_{aij}$ of a dosimeter calibrated accurately in an MRR is the most crucial and key problem (Assiamah et al., 2005, Cabal and Kluson, 2010).

## 2. CAK determination method in an MRR

MRR is a cubic and closed space shielded with lead plates and an isotope cesium-137 irradiator acts as the gamma-ray source. Its geometric center is defined as the point of test, at which the reference

* Corresponding author.
*E-mail addresses:* liuyx123456789@126.com (Y. Liu), gena@vip.sina.com (B. Mao).

http://dx.doi.org/10.1016/j.apradiso.2016.09.018
Received 22 October 2015; Received in revised form 2 September 2016; Accepted 14 September 2016
Available online 15 September 2016

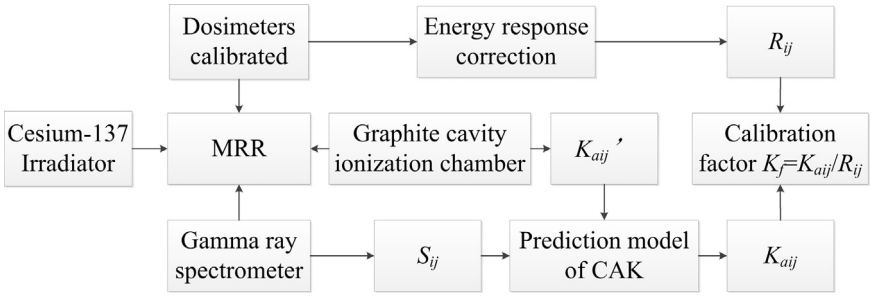


**Fig. 1.** Procedure of calibrating dosimeters based on an MRR.

point of a dosimeter's probe is positioned. Because of the scattering ray produced by the inner shielding wall and the outer surface of a dosimeters probe calibrated inside the MRR, the gamma-ray composition irradiating on a dosimeter's probe at the point of test is different from that in an SRR. Therefore, the air kerma value $K_{aij}'$ measured by a graphite cavity ionization chamber at the point of test is not the CAK defined by the ISO 4037 series, because the CAK is a quantity binding an SRR (Burns, 2006, Burns et al., 2007). $K_{aij}'$ is not only the response of gamma ray originating directly from the irradiator, but also the response of scattering ray, and both of them are related closely to the gamma-ray intensity from the radioactive source in the irradiator. Therefore, $K_{aij}'$ can be used to characterize the irradiating gamma-ray intensity during calibration. To obtain the information of scattering ray, a gamma-ray spectrometer was used and its probe was placed in the MRR to monitor the scattering components with a scattering gamma-ray spectrum $S_{ij}$ (Assiamah et al., 2005, Cabal and Kluson, 2010), which was further used to characterize and correct the interference of scattering gamma ray in constructing the CAK prediction model.

Sample dosimeters should be selected carefully for its bridge function in establishing a metrological equivalence between the MRR and SRR, and their performance should be better while their detector types should be the same as or similar to those needed to be calibrated. To measure the scattered spectrum better, the probe of the gamma spectrometer placed in the MRR should not be irradiated directly by gamma ray originating from the irradiator. The CAK determination method and procedure are presented in Fig. 2.

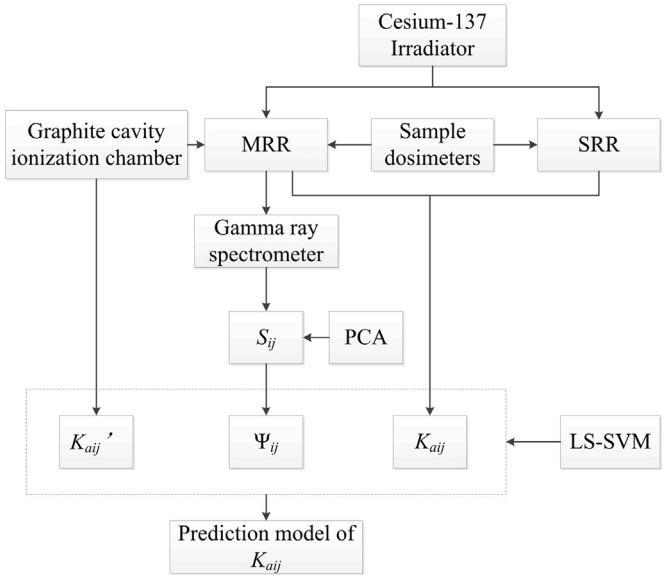


**Fig. 2.** The building procedure of a CAK prediction model at the point of test in an MRR.

### 2.1. Determining the CAKs

For determining $K_{aij}$ at the point of test in an MRR when a sample dosimeter is placed, the sample dosimeter was used as a transfer tool and placed at the point of test in the MRR and SRR. $K_{aij}$ was numerically equal to the CAK at a point in the SRR, where the indication value of the sample dosimeter is equal to that in the MRR. A detailed summary of the procedures is as follows:

First, a sample dosimeter $i$ was placed at the point of test in the MRR, and the indication value of the dosimeter $R_{ij}$ was then obtained by irradiating the dosimeter with a gamma-ray source of intensity $I_j$. Second, the dosimeter $i$ was transferred from the MRR to the SRR of a calibration facility, and a point in the SRR was then found, where the indication value of the sample dosimeter $i$ was equal to $R_{ij}$. The CAK at the point we found in the SRR could be equivalent to the value of $K_{aij}$ at the point of test in the MRR.

With the proposed procedures, the metrological equivalent relationship between an MRR and SRR can be established on the basis of a group of $K_{aij}$ data obtained experimentally with a group of sample dosimeters. It also means that the investigation we carried out and the mobile calibration technology we developed are equivalent to or comply with ISO 4037 series, which depend on the MRR and a group of sample dosimeters (Merimaa et al., 2012).

### 2.2. Building a CAK prediction model

By analyzing the gamma-ray components and their original sources at the point of test in the MRR, we found that the CAK in the MRR can be determined by both scattering spectrum $S_{ij}$ and air kerma value $K_{aij}'$:

$$K_{aij} = f(S_{ij}, K_{aij}') \quad (1)$$

Equation (1) indicates that the CAK or $K_{aij}$ at the point of test in the MRR is contributed by the gamma-ray beam originating directly from the isotope source in the irradiator and the scattering gamma ray caused by the MRR's inner wall and the outer surface of a sample dosimeters probe. Although $S_{ij}$ is not the direct response of the scattering ray at the point of test, it has indirect relationship with the scattering ray at the point of test. Furthermore, it is also the response of original irradiation gamma ray, the dimension and the inner shielding material of the MRR, and the probe size of the sample dosimeters or the calibrated dosimeters.

When $x$ sample meters($i$) and $y$ irradiation gamma-ray intensity($I_j$) are employed simultaneously, $x \times y$ lines of spectrum $S_{ij}$ and $K_{aij}'$ can be obtained. When dispersing each $S_{ij}$ by a fixed gamma-ray energy separation $E$, we may obtain a group of discrete gamma-ray count rate data or a data set $\varphi_{ijn}$, where $n$ is the number of count rate data of $\varphi_{ijn}$. The parameter $\varphi_{ijn}$ corresponds to gamma-ray energy or the channel address of the spectrum line. Then, an $n$-dimensional sample data matrix $\Phi_{(x\times y)\times n}$ can also be constituted by $x \times y$ data sets of $\varphi_{ijn}$. To reduce the dimensions of $\Phi_{(x\times y)\times n}$, the principal component analysis (PCA) was used to extract feature components $\Psi_{ij}$ (Richard et al., 2007; Xu et al., 2014). This significantly simplified the sample data matrix $\Phi_{(x\times y)\times n}$. In general, the dimensional number $n$ was reduced from hundreds to several tens. Therefore, Equation (1) can be simplified as

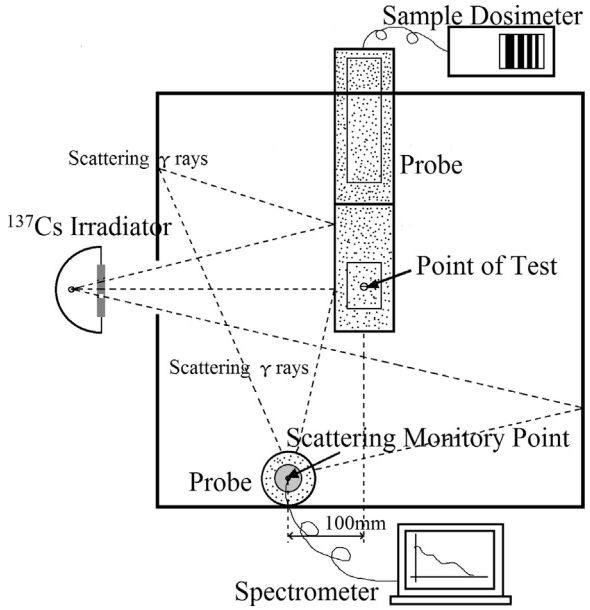


**Fig. 3.** Cross section of layout of the MRR.

Eq. (2):

$$K_{aij} = f(\Psi_{ij}, K_{aij}') \quad (2)$$

On the basis of the feature components $\Psi_{ij}$ extracted from $S_{ij}$ and $K_{aij}'$ measured experimentally, the function relation of Eq. 2 was established by using the least square support vector machine (LS-SVM) to execute the regression fitting (Cristianini and Shawe-Taylor, 2000; Suykens and Vandewalle, 1999). It is the basic mathematical equation of the CAK prediction model at the point of test in an MRR.

In the process of regression fitting, $\Psi_{ij}$ and $K_{aij}'$ are used as input variables while $K_{aij}$ is used as an output variable. An appropriate kernel function should be selected. The sample data and their ratio applied for training and testing separately should be distributed carefully. The whole procedure of acquiring the CAK prediction model is presented in Fig. 2.

## 3. Experimental installation

The MRR used in the investigation is a cubic box of 0.5-m-length and was shielded by 3-mm-thick lead plates. The center of a side had a 120-mm-diameter circular hole, which was used for gamma-ray irradiation. In experiments, the probe of a sample dosimeter could be hanged vertically on a support and inserted into the MRR through a circular hole on the center of the top side of the shielding box. The reference point on the probe was adjusted to coincide with the point of test. A scattering monitory point was labeled for positioning the probe of a gamma-ray spectrometer on the central line of the MRR's inner bottom, near the side of gamma-ray inlet and 100 mm away from the projection point of the point of test (Fig. 3). Fig. 4 illustrates the experimental installation.

The experimental setup was installed in a calibration facility called Gamma-ray air kerma (safety level) measurement standard (briefly called standard installation), which belongs to the Ionization Radiation Metrology Station, a subsidiary institution of China Academy of Engineering Physics. In the MRR, gamma ray was irradiated horizontally from a cesium-137 isotope source with an activity of $7.14\times10^{10}$ Bq in the irradiator of the standard installation (Ross and Grosswedt, 1987). To investigate the effect of gamma-ray intensities, gamma-ray attenuators with different attenuation ratio could be assembled in the outlet of the irradiator. At the same time, the distance between the outlet of the irradiator and the MRR box placed on a small rail car could also be changed to adjust irradiating gamma-ray intensity.

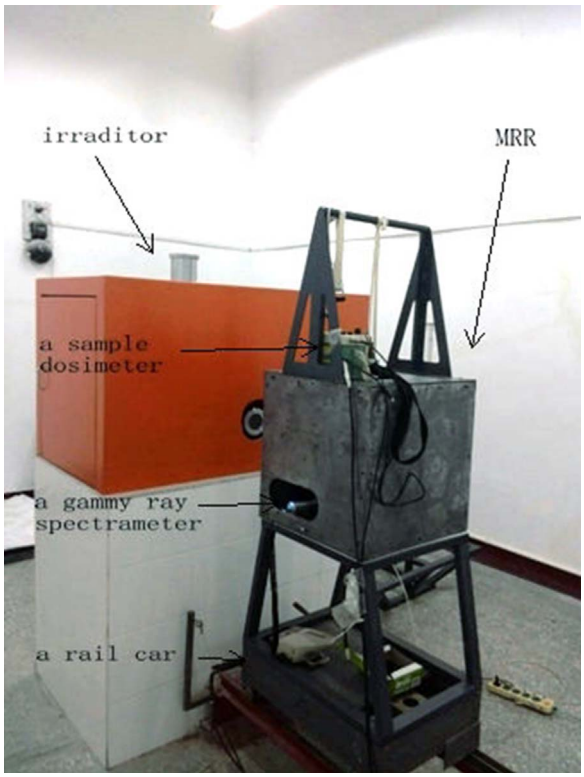


**Fig. 4.** Experimental installation.

According to the regulated dose rate range that is within the safety level, we set four gamma-ray intensities $I_j$ ($j$=1, 2, 3, 4) for investigation by using different attenuators and adjusting the distance between the MRR and the irradiator. The dose rates at the point of test corresponding to each intensity (also called each source) we investigated are presented in Table 1.

During experiments, a calibrated graphite cavity ionization chamber (model PTW-32005, PTB, Germany) was used to determine the air kerma value at the point of test. A portable gamma-ray spectrometer (Model InSpector 1000, Canberra, USA) was used to monitor the scattering gamma ray in the MRR. The entire investigation was carried out with four gamma-ray intensities and 12 sample dosimeters, including two types of detectors. Details of the sample dosimeters are presented in Table 2. Finally, 41 sets of effective sample data were acquired, except those in which the irradiating dose rates were over the range of the sample dosimeter. Each data set includes $S_{ij}$ at the scattering monitory point measured by the spectrometer InSpector 1000, $K_{aij}'$ measured by the graphite cavity ionization chamber PTW-32005, and CAK or $K_{aij}$ at the point of test acquired through the procedures described above.

## 4. Result and discussion

### 4.1. Characteristics of scattering ray

When seven sample dosimeters probes were placed into the MRR one by one and irradiated with source 4, seven spectra $S_{ij}$ were obtained as shown in Fig. 5. There were five characteristic peaks appearing in each spectrum line, and all the emerging peak positions were almost the same for each spectrum line. In Fig. 5, the count rates of four left peaks presented an increasing trend with the increase in the probe diameter, except peak 5. As shown in Fig. 6, peaks 1 and 4 seemed to be affected more seriously by the increase in probe diameters, and peak 4 in particular seemed more sensitive than other peaks. The gamma-ray energy of peak 1 is approximately 77 keV, which corresponded to the characteristic X-ray energy of cesium-137 gamma ray interacting with

**Table 1**
Dose rates investigated at the point of test.

| Number of source | Source 1 | Source 2 | Source 3 | Source 4 |
|---|---|---|---|---|
| Dose rate(μGy/h) | 67.68 | 148.68 | 393.48 | 894.24 |

the lead shielding walls (Fernandes et al., 2004). According to the irradiation geometry in Fig. 3, we can calculate the scattering ray energy using the following equation:

$$hv' = \frac{hv}{1 + (hv/mc^2)(1 - \cos\varphi)} \quad (3)$$

Then, we found that the energy of peak 3 was approximately 195 keV, which was mainly from the Compton scattering of irradiating gamma ray interacting with the opposite inner lead walls. The energy of peak 4 was approximately 239 keV, and it corresponded to the Compton scattering gamma-ray energy value that originated mainly from the mutual interaction of irradiation gamma ray with the surface of the sample dosimeter probe (Rogers, 1987). Peak 2, at approximately 141 keV, was mainly due to the Compton scattering in measuring irradiation gamma ray with the spectrometer.

The above results coincided with the Monte Carlo simulation shown in Fig. 7 (Kim, 2016). The energy of peak 5 is approximately 625 keV, which resulted from the attenuation and scattering of incident gamma ray of cesium-137 source through the MRR's thin lead wall. Compared with Figs. 5 and 6 does not have peak 5 emerging in the scattering spectrum. This is because the simulative incident gamma ray was assumed to be shielded totally by the thick shielding wall.

When irradiated with all four sources and using only one BH3103A dosimeter with a probe diameter of 93 mm, we obtained four spectra, as shown in Fig. 8. The positions of left four peaks were almost the same and the shapes of each spectrum lines were quite similar, as shown in Fig. 5. The peak count rates obviously increased with the intensity of gamma-ray irradiation, as shown in Fig. 9. Therefore, we found that irradiation gamma-ray intensities had more serious impact on the peak count rates than probe diameter.

A significant difference in peak 5 was found Figs. 5 and 8, regardless of the positions or the peak heights. The difference in peak heights should be attributed to the different irradiation source intensities. The difference in position is mainly due to the inaccurate manual positioning of the MRR on the rail car of the irradiator and the relative experimental errors.

Two feature components were acquired by PCA and shown in Fig. 10, which were applied to substitute the seven scattering gamma ray spectra in Fig. 5. The first component occupies 86.26% information of the original data, while the second occupies only 9.1%. We found that the left four peak shapes of the first feature component are very similar to those in the original scattering gamma-ray spectra illustrated in Fig. 5, except the rightmost peak. This might be a proof that the first feature component contains most information of original scattering gamma-ray spectra. However, the curve of the second feature component has acute variation corresponding to the positions of peaks 1, 4, and 5. This might imply that probes and sources had more information

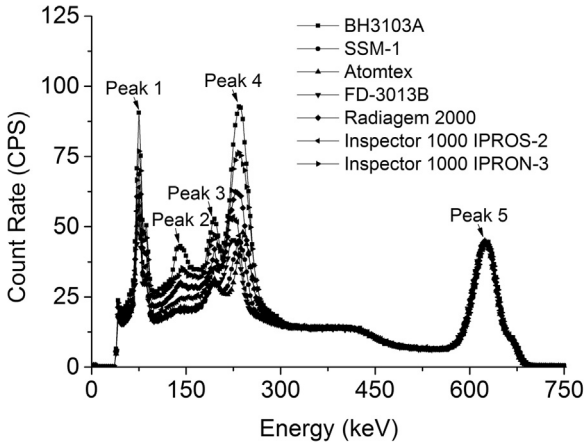


**Fig. 5.** Scattering gamma ray spectra of seven probes irradiated with source 4.

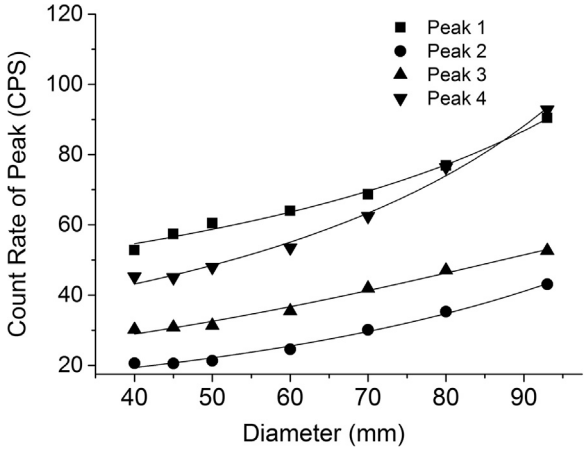


**Fig. 6.** Relationship between peak count and probe diameter.

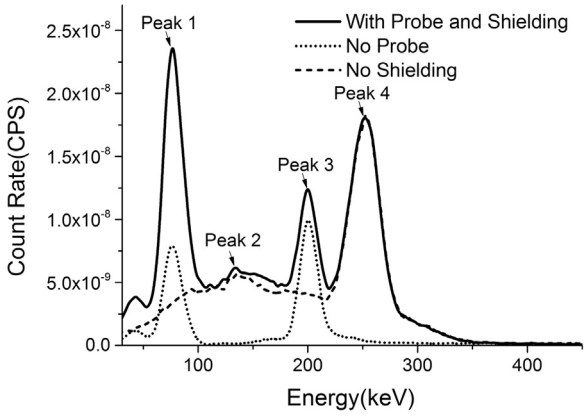


**Fig. 7.** Scattering gamma ray spectra in an MRR simulated by Monte Carlo tool MCNP.

**Table 2**
Sample dosimeters used for investigation.

| SN | Model | Probe diameter | Detector type | Amount | Manufacturer |
|---|---|---|---|---|---|
| 1 | BH3103A | 93 mm | NaI | 3 | Beijing Nuclear Instrument Factory |
| 2 | SSM-1 | 45 mm | GM | 3 | Austrian Research Center Seibersdorf |
| 3 | ATOMTEX AT6130 | 50 mm | GM | 2 | Scientific and Product Enterprise, Belarus |
| 4 | FD-3013B | 40 mm | NaI | 1 | CNNC Shanghai Electronics Instrument Co., Ltd., China |
| 5 | Radiagem 2000 | 70 mm | NaI | 1 | Canberra USA |
| 6 | Inspector1000 IPROS-2 | 60 mm | NaI | 1 | Canberra USA |
| 7 | Inspector1000 IPRON-3 | 80 mm | NaI | 1 | Canberra USA |

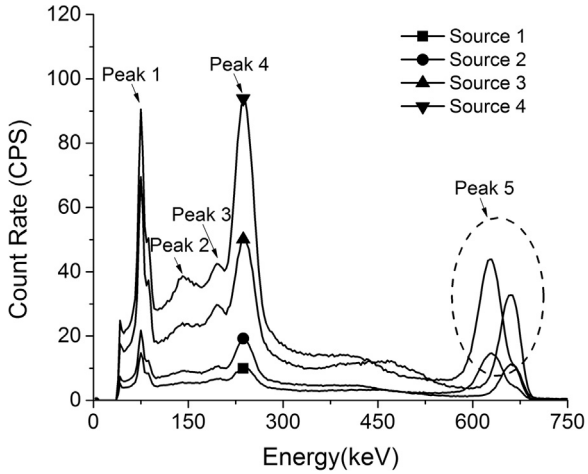


**Fig. 8.** Scattering gamma spectra of BH3103A when irradiated with four sources.

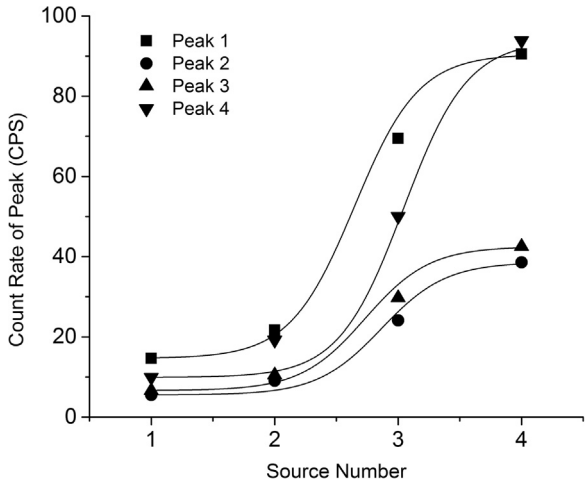


**Fig. 9.** Relationship between peak count rate and source intensity.

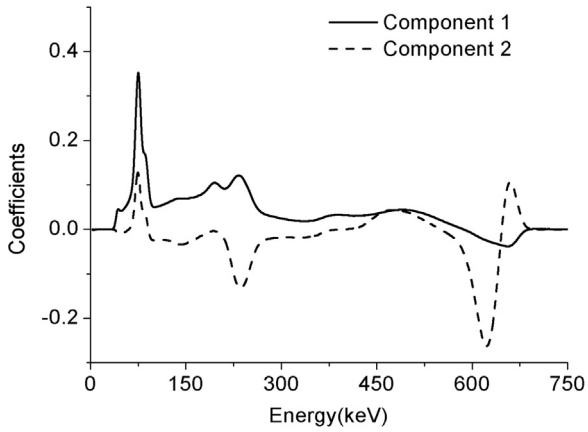


**Fig. 10.** Feature components of scattering gamma spectrums for source 4 and seven sample dosimeters.

than were present at peaks 2 and 3.

The feature components of the four scattering gamma-ray spectra in Fig. 8 are shown in Fig. 11. The first component contained 86.24% of the information, while the second component contains only 8.43%. There was a clear distinction in the curve's shapes from the original spectra of the curve of the first feature component. There were no peaks emerging at the position of peak 3 correspondingly, as illustrated in Fig. 12, which might mean that peak 3 on the original scattering gamma-ray spectra responded mainly to the probe physical size rather

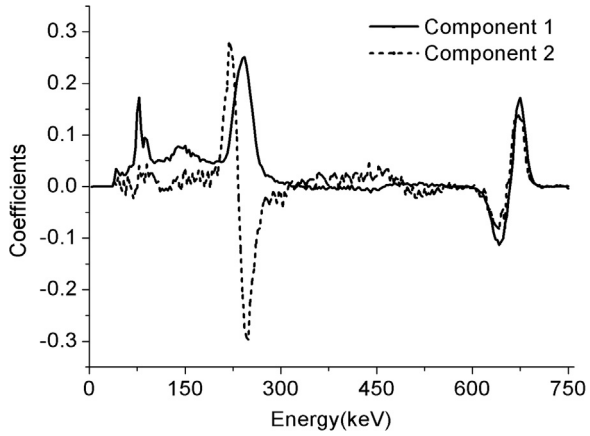


**Fig. 11.** Feature components of scattering gamma-ray spectra for four sources.

than the irradiation source intensities. There was obvious and acute variation in the curves of both feature components at the corresponding position of peak 4, which might indicate that peak 4 is also sensitive to irradiation sources or gamma-ray irradiation intensity, in the same way as those at the position of peak 5.

According to the above investigation and discussion, we found that all characteristic peaks on the scattering spectrum, except peak 5, are attributed to both gamma-ray irradiation and probe diameter. Compared to probe diameter, gamma-ray intensity may obviously increase the height of peaks. Peak 4 seems more sensitive to probe size, while peak 3 responds to the contribution of probe size more purely. Peaks 1 and 5 rely strongly on the intensity of gammy-ray irradiation. We also found that feature components can contain almost total characteristics of original scattering gamma-ray spectra and reflect some information, which the scattering gamma-ray spectra do not contain. Through feature component curves, we can recognize more clearly the elements contributing to the characteristic peaks on scattering gamma-ray spectra and even the components that disturb the minitype radiation field and not just scattering gamma-ray spectra themselves. PCA is a useful and effective tool that can reduce the amount of data significantly from scattering gamma-ray spectra.

### 4.2. CAK prediction model and results

When dispersing a $S_{ij}$ line with a constant gamma-ray energy separation of 3 keV, a 250-dimensional data matrix $\Phi_{48\times250}$ was obtained for four sources and 12 sample dosimeters. The data with gamma-ray energy > 750 keV were abandoned because of absence of obvious characteristics. Unfortunately, a part of data were invalid because the measured values were over the indication range of sample dosimeters; therefore, only 41 of 48 groups of the data were effective and used. After extracting feature components from $S_{ij}$ by PCA, two feature components $\Psi_{ij}$ were obtained with the factor $\delta_n$ of 90%, and the 250-dimensional data matrix $\Phi_{41\times250}$ was simplified to $\Phi_{41\times2}$.

The LS-SVM toolbox in MATLAB software was used for regression of CAK prediction model based on the data matrix $(K_{aij}, \Psi_{ij}, K_{aij}')_{41\times(p+2)}$, where $p$ is the amount of feature components extracted by PCA, which equals 2 here. During the course of regression, the data matrix was divided into training and testing sets. The kernel function was selected and used the radial basis function (RBF) as given in Eq. (4) (Çalişir and Dogantekin, 2011):

$$K(x, x_i) = \exp\left(-\frac{\|x - x_i\|^2}{2\sigma^2}\right) \tag{4}$$

where $x_i$ is the center of the kernel function and $\sigma^2$ is the width parameter of the kernel function. In the course of training, the width parameter $\sigma^2$ and another parameter called regularization parameter $c$, which affects the effect of regression, were initialized as $\sigma^2 = 0.05$ and

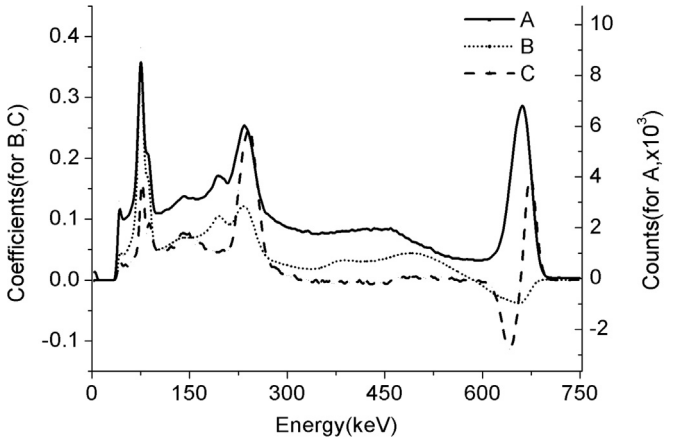


**Fig. 12.** Comparison diagrams of the first feature components extracted in two conditions and the scattering spectrum of a BH3103A dosimeter. Line A is a scattering spectrum of BH3103A irradiated with source 4; Line B is the first component extracted from the scattering spectra when seven sample dosimeters were used and irradiated with source 4; Line C is the first component extracted from the scattering spectra when only a BH3013A dosimeter was used and irradiated with all four sources.

$c$=100. The two parameters were then confirmed through the L-fold cross-validation method, L=10 (Zhang et al., 2013). The CAK prediction model was acquired according to the following formula:

$$K_{aij} = F\,[(\Psi_{ij}, K_{aij}'),\quad (\Psi'), K']' \times \alpha + b, \tag{5}$$

where $F$ is the kernel function for model regression training, $\alpha$ is the regression factor of the model, $b$ is the bias of the model, $\Psi'$ is the sample feature component matrix, and $K'$ is the sample data matrix of $K_{aij}$ (Brabanter et al., 2012). It is an $n$-dimensional vector, where $n$ is the amount of sample data for training the model. To improve the prediction model, we constructed the model through two approaches. One approach was regression fitting of the model by using all sample data, and only one CAK prediction model was obtained and named combined-intensity prediction model (CIPM). The other approach was regression fitting of the model by using the data corresponding to each source separately. Consequently, four CAK prediction models were constructed for our four-source experiment. We named these four CAK prediction models as single-intensity prediction model (SIPM). The parameters of CIPM and SIPM are listed in Table 3.

Error comparison of CAK prediction values by applying the above two types of models is presented in Fig. 13 and Table 4.

Fig. 13 and Table 4 show that all types of errors are within ± 10%. This indicates that this technology is capable of determining the CAK in calibrating a dosimeter by IEC60846 IEC (2002), in which the requirement to the relative intrinsic error index is within ± 20% for a qualified dosimeter calibrated in the field of radiation protection. We also found that SIPM has better prediction accuracy than CIPM. Error percentage of SIPM is lower than CIPM, and only one prediction error is more than 5% for SIPM in 41 sets of sample data. Yet, the prediction accuracy was improved with the increase in gamma-ray irradiation intensity, especially for CIPM. Thus, we can deduce that prediction accuracy of the CAK prediction model can be possibly increased by improving the sample data in the condition of weak gamma-ray irradiation intensity and/or increasing the amount of sample irradiation sources.

## 5. Uncertainty budget

The measurement model of CAK or $K_{aij}$ was presented as Eqs. (1), (2), and (3), and can also be represented as

$$K_{aij} = f\,(S_{ij}, K_{aij}')\cdot N_{er}\cdot N_{ir}\cdot N_{dr}\cdot N_{Tp} \tag{6}$$

where, $N_{er}$ is the correction factor of the energy response of calibrated dosimeters, the graphite cavity chamber, and the gamma-ray spectrometer $N_{ir}$, $N_{dr}$, and $N_{Tp}$ are correction factors of the graphite cavity ionization chamber for its ion recombination, directional response, and air density, respectively. These are the sources of measurement error.

**Table 3**
Parameters of CIMP and SIPM.

| Parameter | CIPM | SIPM | | | |
|---|---|---|---|---|---|
| Source | All Source | Source 1 | Source 2 | Source 3 | Source 4 |
| Dimension of $\alpha$ | 41 | 11 | 10 | 12 | 8 |
| b | 0.3475 | 0.2913 | 0.8796 | 0.1821 | 0.1051 |

In an MRR, the gamma-ray components are obviously different from those in an SRR, and it will change significantly with the variable probe size of calibrated dosimeters. It will be also influenced by the elements related to the irradiation source and the experimental installation assembly, especially for our assorted experimental installation and manual operation way. These are also the sources of measurement error.

The distance between the irradiator and the point of test $D_i$ is directly proportional to the intensity of the gamma rays, and it depends mainly on the positioning of MRR on the rail car. It is an important error source caused by manual positioning. The positioning reproducibility of the isotope source cesium-137 in the irradiator is also an error source, which relates to the reproducibility of gamma-ray irradiation intensity in the MRR. The sample data of $K_{aij}$ and $K_{aij}'$ for the regression of CAK prediction model were measured by the graphite cavity ionization chamber and the sample dosimeters in the MRR and SRR, respectively, and the errors of their indication values caused by radioactive statistical fluctuation and energy response of varied radiation field components in the MRR should not be neglected either. $S_{ij}$ was measured by a gamma-ray spectrometer, and it was also an important error source (Takata et al., 2007).

All error sources mentioned above are the primary error sources for CAK determination related to our investigation. Among them, the indication value errors of dosimeters in the determination of $K_{aij}$ and $K_{aij}'$ were determined by the standard deviation of all measurement data and the maximal values were selected. The errors caused by energy response difference were determined by the maximal energy response index of all detectors involved and treated as uniformity distribution. The positioning errors of $D_i$ and $d_i$ of the geometric position of detectors involved were determined by empirical data. In addition to these error elements, all other errors were determined by their technical specification and treated with uniformity distribution. The uncertainty evaluation complies with the ISO/IEC Guide 98-3-2008, and all primary error sources, uncertainty components, and their budget are presented in Table 4 (ISO/IEC, 2008).

During the course of uncertainty compositing, we treated all components as mutually independent. In fact, some of them are mutually correlative, for example, $K_{aij}$, $K_{aij}'$, and $S_{ij}$ are correlated with gamma-ray irradiation intensity. Therefore, there is a possibility of underestimating measurement uncertainty by our method.

From Table 4, we found that the relative combined standard uncertainty $u_c$ for the CAK determination presented in this study can reach 4.65%, and the relative expanded uncertainty reached 9.30%. This evaluation result of measurement uncertainty coincided with the measurement error within 10% based on all experimental data and the CIPM model. For the SIPM model, the measurement error can reach 5%. This may indicate that irradiation sources or related elements largely contribute to measurement uncertainty. It might also imply that the measurement uncertainty can increase further. In any case, the relative expanded uncertainty of 9.30% we reached shows again that the technology illustrated in this study is capable of meeting the primary requirement of the relative intrinsic error index regulated by IEC 60846 Table 5.

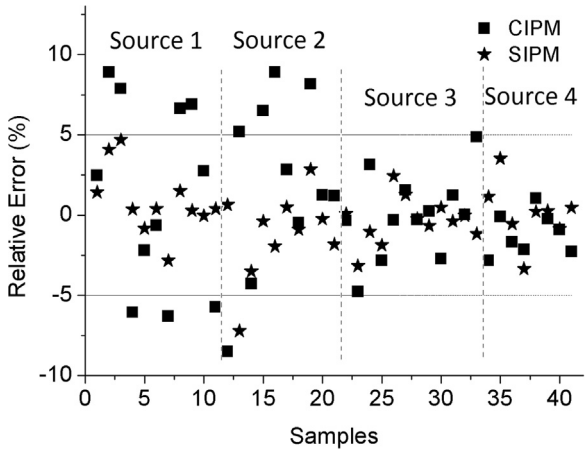


**Fig. 13.** Distribution of the prediction relative errors of CIPM and SIPM.

**Table 4**
Dose rates investigated at the point of test.

| Model Type | SIPM | CIPM |
|---|---|---|
| Maximum training error (%) | 1.82 | 8.52 |
| Mean training error (%) | 0.54 | 2.49 |
| Minimum training error (%) | 0.03 | 0.03 |
| Maximum test error (%) | 7.21 | 8.90 |
| Mean test error (%) | 2.64 | 4.44 |
| Minimum test error (%) | 0.36 | 0.11 |

**Table 5**
Uncertainty factors and budget (%).

| No. | Uncertainty components | Type and Value | |
|---|---|---|---|
| | | Type A | Type B |
| 1 | Indication values of dose meters in $K_{aij}$ and $K_{aij}'$ determination caused by radioactive statistical fluctuation, $N_{iv}$ | 2.89 | 0.00 |
| 2 | Scattering gamma-ray spectrum ($S_{ij}$) measurement, $N_{gs}$ | 0.00 | 2.02 |
| 3 | Errors of dose meters and the gamma-ray spectrometer caused by energy response, $N_{er}$ | 0.00 | 2.89 |
| 4 | Geometric position ($d_i$) of dose meters | 0.00 | 2.89 |
| 5 | Distance between the irradiator and the point of test ($D_i$) | 0.00 | 0.58 |
| 6 | Reproducibility of the cesium-137 source position in the irradiator | 0.00 | 0.30 |
| 7 | Ion recombination of standard graphite cavity ionization chamber, $N_{ir}$ | 0.00 | 0.23 |
| 8 | Air density correction for standard graphite cavity ionizing chamber, $N_{Tp}$ | 0.00 | 0.29 |
| 9 | Relative combined standard uncertainty (%), $u_c$ | 4.65 | |
| 10 | Relative expanded uncertainty (%), $U_{ce}$, (k=2) | 9.30 | |

We also find that $N_{iv}$, $N_{gs}$, and $N_{er}$ are top three and primary uncertainty sources, and they contributed approximately 98% of the uncertainty budget. We evaluated $N_{gs}$ and $N_{er}$ in this study according to the detectors' technical specification and selected the maximal index, and it might be an overestimation. By correcting $K_{aij}$ and $K_{aij}'$ data with detector type and radiation component one by one before constructing the CAK prediction model, the errors of energy response $N_{er}$ might be reduced significantly in further investigation. The measurement precisions of $S_{ij}$, $K_{aij}$, and $K_{aij}'$, which are related to the error components of $N_{iv}$ and $N_{gs}$, will be improved by controlling measurement time and selecting better performance of sample dosimeters, especially in lower irradiation gamma-ray intensities. It is anticipated that the errors caused by the MRR's position ($D_i$) and probe's position ($d_i$) will be improved significantly by a new design and more perfect experimental installation in the future. In fact, the quality of CAK prediction model itself is also an error source of measurement uncertainty that should not be neglected too, and obviously, it will be improved by promoting the construction technique of the CAK prediction model, which needs to be carried out in the future.

## 6. Conclusion

This study showed the feasibility of determining the CAK of a calibrated dosimeter in a 0.5 m×0.5 m×0.5 m MRR. The technology developed in this study may provide a novel way to calibrate fixed and field dosimeters or calibrate dosimeters in a mobile way, which is equivalent to the method regulated in ISO 4037 series relied on an SRR and will meet in principle the regulation requirement of IEC-60846 for radiation protection instrumentation.

Compared with a normal SRR, a small MRR has a weight of several hundred kilograms and dimension of less than 1 m. In an MRR, scattering gamma-ray spectra and their feature components can be used to characterize the probe's interference to the radiation field. PCA is an effective tool to extract scattering features from original scattering gamma-ray spectra. We believe that the use of more typical and large amount of sample dosimeters can enable to extract more representative feature components. Among the two types of CAK prediction models constructed by LS-SVM, SIPM had better CAK prediction accuracy than CIPM and it can reach the best value of 5% relative measurement error. The relative combined standard uncertainty of 4.65% was reached by evaluation, and it might be improved by further work. The scattering gamma-ray spectrum measurement, energy response errors of dosimeters, and their indication value errors are three primary elements influencing the measurement uncertainties, and there are possibilities to improve them in the future.

However, much research needs to be conducted for some dosimeters, especially for those that significantly differ in the type, probe physical dimension, and shape from the sample dosimeters. Briefly, this study showed the feasibility of calibrating fixed or field dosimeters using an MRR, or a mobile way of calibrating dosimeters, which significantly differ from the normal calibration with a fixed SRR.

## Acknowledgements

This study was supported by the Ionization Radiation Metrology Station of China Academy of Engineering Physics (Grant no. INPC20140206009), and part of its employees.

## References

Assiamah, M., Nam, T.L., Keddy, R.J., 2005. Comparison of mammography radiation dose values obtained from direct incident air kerma measurements with values from measured X-ray spectral data. Appl. Radiat. Isot. 62 (4), 551–560.
Brabanter, K.D., Karsmakers, P., Brabanter, J.D., Suykens, J.A.K., Moor, B.D., 2012. Confidence bands for least squares support vector machine classifiers: a regression approach. Pattern Recogn. 45 (6), 2280–2287.
Burns, D.T., 2006. A new approach to the determination of air kerma using primary-standard cavity ionization chambers. Phys. Med. Biol. 51 (4), 929–942.
Burns, D.T., Kessler, C., Roger, P., 2007. Air-kerma determination using a variable-volume cavity ionization chamber standard. Phys. Med. Biol. 52 (23), 7125–7135.
Cabal, G., Kluson, J., 2010. Air Kerma Rate estimation by means of in-situ gamma spectrometry: a bayesian approach. Appl. Radiat. Isot. 68 (4–5), 804–806.
Çalişir, D., Dogantekin, E., 2011. A new intelligent hepatitis diagnosis system: PCA-LSSVM. Expert. Syst. Appl. 38 (8), 10705–10708.
Cristianini, N., Shawe-Taylor, J., 2000. An Introduction to Support Vector Machines and Other Kernel Based Learning Methods. Cambridge university press.
Fernandes, E., Freire, D., de Freitas, A.C., Dealmeida, C.E., 2004. The radiation field characteristics of a $^{137}$Cs source used for calibration of radiation protection instruments. Appl. Radiat. Isot. 61 (6), 1425–1430.
IEC, 2002. Radiation protection instrumentation-Ambient and/or directional dose equivalent (rate) meters and /or monitors for beta, X and gamma radiation.
ISO/IEC, 2008. Uncertainty of Measurement-part 3: Guide to the expression of uncertainty in measurement, ISO/IEC Guide 98-3-2008.
ISO-4037-1:1996, 1996. X and gamma reference radiation for calibration dosimeters and

dose rate meters and for determining their response as a function of photo energy-Part 1: Radiation characteristics and production methods, Geneva.
ISO-4037-2:1997, 1997. X and gamma reference radiation for calibration dosimeters and dose rate meters and for determining their response as a function of photo energy – Part 2: Dosimetry for radiation protection over the energy ranges 8 keV to 1.3 Mev and 4 MeV to 9 MeV, Geneva.
JJG393-2003, 2003. X and Gamma Radiation Dose Equivalent (Rate) Meters and Monitors Used in Radiation Protection.
Kim, S., 2016. Gamma radiation transmission along the multibend mazes. Appl. Radiat. Isot. 114, 45–49.
Merimaa, K., Tapiovaara, M., Kosunen, A., 2012. Calibration and features of air-kerma length product meters. Radiat. Prot. Dosim. 152 (4), 384–392.
Minniti, R., Seltzer, SM., 2007. Calibration of a $^{137}$Cs $\gamma$-ray beam irradiator using large size chambers. Appl. Radiat. Isot. 65 (4), 401–406.
Richard, A Johnso, Dean W.W., 2007. Applied Multivariate Statistical Analysis. Pearson Education.
Rogers, D.W.O., 1987. Introduction to radiological physics and radiation dosimetry: by F.H.Attix. Med. Phys. 14 (4), 692.
Ross, M., Grosswedt, B., 1987. A simplified method for large-range variations of dose rate for $^{137}$Cs gamma radiation. Radiat. Prot. Dosim. 18 (3), 147–151.
Suykens, J.A.K., Vandewalle, J., 1999. Least squares support vector machines classifiers. Neural Process. Lett. 9 (3), 293–300.
Takata, N., Kurosawa, T., Begum, A., Sugita, T., 2007. Physical parameters and correction factors for ionization chambers for absolute measurement of air kerma in $\gamma$-ray fields. Nucl. Instrum. Methods Phys. Res. Sect. A 580 (580), 346–349.
Xu, X., Xie, L., Wang, S., 2014. Multimode process monitoring with PCA mixture model. Comput. Electr. Eng. 40 (7), 2101–2112.
Zhang, Y., Qin, Y., Xing, Z.Y., Jia, L.M., Cheng, X.Q., 2013. Roller bearing safety region estimation and state identification based on LMD-PCA-LSSVM. Measurement 46 (3), 1315–1324.